

Exploring hybrid equation of state with constraints from tidal deformability of GW170817

Qing-Wu Wang,^{1,*} Chao Shi,^{2,†} Yan Yan,^{3,‡} and Hong-Shi Zong^{4,5,6,§}

¹College of Physics, Sichuan University, Chengdu 610064, China

²Department of nuclear science and technology, Nanjing University of Aeronautics and Astronautics, Nanjing 210016, China;

³School of Mathematics and Physics, Changzhou University, Changzhou, Jiangsu 213164, China

⁴Department of Physics, Nanjing University, Nanjing 210093, China

⁵Department of Physics, Anhui Normal University, Wuhu, Anhui 241000, China

⁶Nanjing Institute of Proton Source Technology, Nanjing 210046

With a interpolation method on the P - μ plane, a hybrid equation of state is explored. The quark phase is described by our newly developed self-consistent two-flavor Nambu–Jona-Lasinio model. It retains the contribution from the vector channel in the Fierz-transformed Lagrangian by introducing a weighting parameter α [Chin. Phys. C **43**, 084102 (2019)]. In the hadron phase we use the relativistic mean-field theory. We study the dependence of hybrid EOS and mass-radius relation on α . It is found that increasing α makes the hybrid EOS softer in the medium pressure. We can get stellar mass larger than $2M_{\odot}$. Further, we calculate the tidal deformability $\tilde{\Lambda}$ for binary stars and compare with recent analysis GW170817 [Phys. Rev. X **9**, 011001 (2019)].

I. INTRODUCTION

The phase transition of strongly interacting matter is an important topic in hadron physics. As the temperature and density increase, the strongly interacting matter will undergo a phase transition from hadronic phase to quark-gluon plasma (QGP), which is deconfined, approximate chiral symmetric state, superfluid and superconductivity, etc [1–3]. It is generally believed that quarks exist in a hadronic state within a few times the saturation density of nuclear matter. However, how many times is still an open question. This is due to our lack of limited density experimental data. From quark phase to hadron phase, the transition at high temperature and low density may occur as a crossover [4–7]. But whether there is a first-order phase transition at zero temperature and high density or not, along with the existence of the critical end point are still very unclear. Many works indicate that a quarkyonic zone (chiral symmetry is partly restored but quark is still confined) may exist in the phase diagram [8–10]. If so, it will affect chemical equilibrium at the hadron-quark phase transition. Unfortunately, the lattice simulation at present is not successful in exploring high chemical potential regions. What’s more serious is that experiments on Earth in the foreseeable future will have difficulty entering high density.

The boom in the astronomical observations of pulsars and neutron star mergers provides the possibility to check theoretic models of hadron physics. Phase transition in neutron stars has links to gravitational waves [11–13]. Astronomically, it is not easy to determine if phase transitions happened in the inner core of compact stars. Massive stars with quark core are possibly less abundant in the first place. If the observed pulsars are only pure neutron stars or quark stars, there is no possibility to observe any effect of hadron-quark phase transition. In addition, the hadron-quark tran-

sition could also be a crossover at low temperature and high density. In Ref. [14], a peak of postmerger gravitational waves frequency (f_{peak}) is used to identify a first-order phase transition in the interior of neutron stars. But it requires highly precise measurements of the masses and tidal deformabilities.

The discovery of high-mass neutron stars has eliminated a lot of models that provided soft equation of state (EOS) [15–19]. Without modification in the Tolman-Oppenheimer-Volkoff (TOV) equations, only a sufficiently stiff equation of state can support high-mass neutron star. It has been previously thought that stable quark matter should contain strange quarks [20–22], and strange quark stars has become a hot issue. Recent studies have shown that the two-flavor light quark matter can still exist stably [23, 40]. On the other hand, the introduction of strange hadrons will soften the EOS which makes it hard to obtain high-mass compact star [25–27]. It is reasonable to construct a hybrid EOS not containing strange quarks. In Ref. [28], the authors have found that only data from GW170817 [29] is compatible with the existence of hybrid stars.

Two methods are usually used in constructing the hadron-quark phase transition EOS [30–32], i.e., the Maxwell construction and the Gibbs construction. In the Maxwell construction separate neutrality of electric charge is required for the phase transition, but the energy and baryon densities can take different values. It always results in a first-order phase transition and may lead to mass-twin stars [33–35]. In contrast, for the Gibbs construction global neutrality of electric charge is required. Phase transition occurs in a broad area with smoothly increasing of energy density and baryon density.

The EOS from Maxwell construction can get smoothed by pasta structures in the mixed phase with sigmoid function $f_{\pm}(p)$. The parametrization of the EOS is

$$\varepsilon(p) = \varepsilon_h(p)f_-(p) + \varepsilon_q(p)f_+(p). \quad (1)$$

Here, $\varepsilon(p)$ is energy density in the mixed EOS while $\varepsilon_h(p)$ and $\varepsilon_q(p)$ are the energy densities in the hadronic and quark matter phases, respectively. With this smooth EOS, ‘mass-twin’ phenomenon may also exist [36]. In this paper, we try

*Electronic address: qw.wang@scu.edu.cn

†Electronic address: shichao0820@gmail.com

‡Electronic address: 2919ywhhxh@163.com

§Electronic address: zonghs@nju.edu.cn

to use a different interpolation method in exploring the hybrid EOS. The hybrid EOS is derived with a sigmoid interpolating function $f_{\pm}(\mu)$ which we will give later. The energy combination is dependent on the baryon chemical potential with a term $\Delta\varepsilon$ to guarantee thermodynamic consistency

$$\varepsilon(\mu) = \varepsilon^H(\mu)f_-(\mu) + \varepsilon^Q(\mu)f_+(\mu) + \Delta\varepsilon. \quad (2)$$

Here, $\varepsilon(\mu)$ is the total energy density while $\varepsilon^H(\mu)$ and $\varepsilon^Q(\mu)$ are the energy densities of hadron and quark matter respectively. In this method, two parameters μ_c and Γ need to be set at the beginning. The μ_c is the central baryon chemical potential and Γ is half of the interpolating interval at the phase transition area. Out of the interpolating interval, the phases in the low and high chemical potential range are purely hadron and quark phase, respectively.

In Ref.[37], an additional term related to speed of sound c_{QM} in the quark matter is added in the energy density of quark phase

$$\varepsilon(P) = \varepsilon^H(P) + \Delta\varepsilon + c_{QM}^{-2}(P - P_{trans}) \quad (3)$$

when pressure P is larger than the transition pressure P_{trans} . Other method to link the hadron and quark phase with first order phase transition can be found in Refs. [38, 39], where the the combination of pressure is treated as a function that depends on the positions of the end point of hadron phase and the start point of quark phase in the P - ρ or P - μ plane.

At the quark level, we will use our new self-consistent mean-field approximation model [40–43]. Based on the Nambu–Jona-Lasinio (NJL) model and its Fierz-transformation, a parameter α is introduced to weight the contribution from Fierz-transformation Lagrangian. Here α in some sense is like the η in Ref. [32] to count on the vector channel strengths but the way of introduction is totally different. We can adjust α to get stiffer EOS of the quark matter and obtain quark star mass larger than $2 M_{\odot}$. By adjusting weighting parameter α and the vacuum pressure of quark matter we will get the hybrid EOS and compare it with the latest astronomical observation data by calculating the mass-radius relation and tidal deformability.

This paper is organized as follows: In Sec. II, we introduce the Walecka’s nonlinear relativistic mean-field model and our newly developed self-consistent mean-field theory of the NJL model. Then we give our construction for hybrid EOS. In Sec. III, We give our numerical results and analysis on the phase transition. The mass-radius relations are calculated and results are compared with the newly observed high-mass stars. Sec. IV is a short summary of our work.

II. QUARK AND HADRON MODELS

In construction of EOS of hybrid star, we need on one hand models for quark and hadron phases respectively, and on the other hand a method to connect the EOS of quark and hadron phases. In this paper, Walecka’s relativistic mean-field (RMF) theory is used to describe the hadronic state and the recently developed two-flavor NJL model is used to study the

quark state [40–43]. The envelope of the compact object is described by the EOS of Baym-Pethick-Sutherland [44] and Negele-Vautherin [45].

A. The nonlinear $\sigma - \omega - \rho$ model

The nonlinear RMF approach has widely being used in descriptions of nuclear matter and finite nuclei [30, 46]. In the RMF model, the nucleon-nucleon interaction is modelled by the exchanging of σ , ω and ρ mesons. Leptons are added in a β -equilibrium system to keep chemical equilibrium and charge neutrality. In the simplest n - p - e system, the effective Lagrangian can be written as:

$$\begin{aligned} \mathcal{L} = & \bar{\Psi}[i\gamma_{\mu}\partial^{\mu} - M + g_{\sigma}\sigma - g_{\omega}\gamma_{\mu}\omega^{\mu} - g_{\rho}\gamma_{\mu}\tau_i \cdot \rho_i^{\mu}]\Psi \\ & + \frac{1}{2}(\partial_{\mu}\sigma\partial^{\mu}\sigma - m_{\sigma}^2\sigma^2) - \frac{1}{3}g_2\sigma^3 - \frac{1}{4}g_3\sigma^4 \\ & + \frac{1}{2}m_{\omega}^2\omega_{\mu}\omega^{\mu} - \frac{1}{4}\omega_{\mu\nu}\omega^{\mu\nu} + \frac{1}{4}c_3(\omega_{\mu}\omega^{\mu})^2 \\ & + \frac{1}{2}m_{\rho}^2\rho_{i\mu}\rho_i^{\mu} - \frac{1}{4}\rho_{i\mu\nu}\rho_i^{\mu\nu} + \bar{\Psi}_e[i\gamma_{\mu}\partial^{\mu} - m_e]\Psi_e, \end{aligned} \quad (4)$$

where $\omega_{\mu\nu}$ and $\rho_{\mu\nu}$ are the antisymmetric tensors of vector mesons

$$\omega_{\mu\nu} = \partial_{\mu}\omega_{\nu} - \partial_{\nu}\omega_{\mu}, \quad (5)$$

$$\rho_{i\mu\nu} = \partial_{\mu}\rho_{i\nu} - \partial_{\nu}\rho_{i\mu}. \quad (6)$$

In the mean-field approximation, the Euler-Lagrange equations reduce to simpler forms which depend on the ground state expectations of nucleon currents. Meson fields are replaced by their expectation values. The nucleons and leptons are considered as ideal Fermi gas, and then the requirement of charge neutrality $\rho_p = \rho_e$ gives $\mu_p = \mu_e$. Combining with the β equilibrium ($\mu_n = \mu_p + \mu_e$), there is only one free parameter (baryon chemical potential μ_B or baryon number density $\rho^H = \rho_p + \rho_n$) in solving the Euler-Lagrange equations which gives the EOS of the hadronic system. The energy density and pressure of nuclear matter are written as

$$\begin{aligned} \varepsilon^H = & \sum_{B=n,p} \frac{1}{\pi^2} \int_0^{k_F^B} \sqrt{k^2 + m^{*2}} k^2 dk \\ & + \frac{1}{2}m_{\sigma}^2\sigma^2 + \frac{1}{3}g_2\sigma^3 + \frac{1}{4}g_3\sigma^4 + \frac{1}{2}m_{\omega}^2\omega^2 \\ & + \frac{1}{4}c_3\omega^4 + \frac{1}{2}m_{\rho}^2\rho^2 + \frac{1}{\pi^2} \int_0^{k_F^e} \sqrt{k^2 + m_e} k^2 dk, \end{aligned} \quad (7)$$

$$\begin{aligned} P^H = & \sum_{B=n,p} \frac{1}{3\pi^2} \int_0^{k_F^B} \frac{k^4}{\sqrt{k^2 + m^{*2}}} dk \\ & - \frac{1}{2}m_{\sigma}^2\sigma^2 - \frac{1}{3}g_2\sigma^3 - \frac{1}{4}g_3\sigma^4 + \frac{1}{2}m_{\omega}^2\omega^2 \\ & + \frac{1}{4}c_3\omega^4 + \frac{1}{2}m_{\rho}^2\rho^2 + \frac{1}{3\pi^2} \int_0^{k_F^e} \frac{k^4}{\sqrt{k^2 + m_e}} dk, \end{aligned} \quad (8)$$

where $m^* = M - g_\sigma \sigma$ is the nucleon effective mass, k_F is Fermi momentum and all meson fields (σ , ω , ρ) denote their mean-field values.

There are many set of parameters in the RMF theory. We have tried the two typical sets of parameters, NL3 [47] and TM1 [48]. We found only the NL3 parameters is suitable in our construction of quark-hadron hybrid EOS. With a saturation density $\rho_0 = 0.148 \text{ fm}^{-3}$, the NL3 parameters are $m_N = 939.0 \text{ MeV}$, $m_\sigma = 508.194 \text{ MeV}$, $m_\omega = 782.501 \text{ MeV}$, $m_\rho = 763.0 \text{ MeV}$, $g_\sigma = 10.217$, $g_\omega = 12.868$, $g_\rho = 4.474$, $g_2 = -10.431 \text{ fm}^{-1}$, $g_3 = -28.885$, $c_3 = 0$. For a proton-neutron star with these parameters and without considering the EOS of outer crust, the maximum mass of neutron star is about $2.76 M_\odot$ with radius about 12.66 km. If one considers hyperons in the Lagrangian, the coupling between hyperons and mesons must be considered and the EOS will be softened. The hyperons will not be considered in this work since we only consider a non-strange star. Therefore for the quark matter we will also use a two-flavor model.

B. NJL model

We investigate the deconfined quark matter within our newly developed NJL model [40–43]. The NJL model is originally a model of interacting nucleons but later used for quarks. It works in the regions where perturbative QCD is not accessible [1, 49, 50]. The simplest form of NJL Lagrangian includes only the scalar and pseudo-scalar four-quark interactions. Its Fierz-transformation is just a rearrangement of fermion field operators. They can be written as

$$\mathcal{L}_{NJL} = \bar{\psi}(i\partial - m)\psi + G[(\bar{\psi}\psi)^2 + (\bar{\psi}i\gamma^5\vec{\tau}\psi)^2], \quad (9)$$

and

$$\begin{aligned} \mathcal{L}_{Fierz} = & \bar{\psi}(i\partial - m)\psi + \frac{G}{8N_c}[2(\bar{\psi}\psi)^2 + 2(\bar{\psi}i\gamma^5\vec{\tau}\psi)^2 \\ & - 2(\bar{\psi}\vec{\tau}\psi)^2 - 2(\bar{\psi}i\gamma^5\psi)^2 - 4(\bar{\psi}\gamma^\mu\psi)^2 \\ & - 4(\bar{\psi}\gamma^\mu\gamma^5\psi)^2 + (\bar{\psi}\sigma^{\mu\nu}\psi)^2 - (\bar{\psi}\sigma^{\mu\nu}\vec{\tau}\psi)^2], \end{aligned} \quad (10)$$

where m is the current quark mass, G is the four-quark effective coupling, and N_c is the number of color. Since the two forms are equivalent under Fierz-transformation, they can be linearly combined with complex α :

$$\mathcal{L}_C = (1 - \alpha)\mathcal{L}_{NJL} + \alpha\mathcal{L}_{Fierz}. \quad (11)$$

In the mean-field approximation at finite density,

$$\langle \mathcal{L}_{NJL} \rangle = \bar{\psi}(i\partial - m)\psi + 2G\sigma_1\bar{\psi}\psi + \mu\psi^\dagger\psi, \quad (12)$$

$$\begin{aligned} \langle \mathcal{L}_{Fierz} \rangle = & \bar{\psi}(i\partial - m)\psi + \frac{G}{2N_c}\sigma_1\bar{\psi}\psi + G\sigma_1^2 \\ & + \mu\psi^\dagger\psi - \frac{G}{N_c}\sigma_2\psi^\dagger\psi + \frac{G}{2N_c}\sigma_2^2. \end{aligned} \quad (13)$$

Here a term $\mu\psi^\dagger\psi$ is added in both Lagrangians, with chemical potential μ associated with quark number density. The two-quark condensate $\langle \bar{\psi}\psi \rangle$ is denoted as σ_1 and $\sigma_2 = \langle \psi^\dagger\psi \rangle$. From Eqs. (11–13), the effective quark mass and chemical potential are defined respectively, as

$$M = m - 2G'\sigma_1, \quad (14)$$

$$\mu_r = \mu - \frac{G'}{N_c} \frac{\alpha}{1 - \alpha + \frac{\alpha}{4N_c}} \sigma_2. \quad (15)$$

Here G' is the four-quark effective coupling for the mixed Lagrangian Eq. (11) which has the relation with G

$$G' = (1 - \alpha + \frac{\alpha}{4N_c})G. \quad (16)$$

The new coupling G' needs to be recalibrated to fit the low energy experimental data. In the proper-time regularization, the quark condensate is given by

$$\begin{aligned} \langle \bar{\psi}\psi \rangle = & -2N_c \sum_{u,d} \int \frac{d^3p}{(2\pi)^3} \frac{M}{E_p} (1 - \theta(\mu - E_p)) \\ = & -2N_c \sum_{u,d} \left(\int \frac{d^3p}{(2\pi)^3} \int_{\tau_{UV}}^\infty d\tau \frac{e^{-\tau E^2}}{\sqrt{\pi\tau}} \right. \\ & \left. - \int \frac{d^3p}{(2\pi)^3} \frac{M}{E_p} \theta(\mu_r - E_p) \right), \end{aligned} \quad (17)$$

where τ_{UV} is introduced to regularize the ultraviolet divergence, and $E_p = \sqrt{\vec{p}^2 + M^2}$ defines the particle energy. Three parameters (m , G' , and τ_{UV}) are fixed by fitting to the Gell-Mann–Oakes–Renner relation: $-2m\langle \bar{\psi}\psi \rangle = (f_\pi m_\pi)^2$. Here, $f_\pi = 93 \text{ MeV}$, $m_\pi = 135 \text{ MeV}$, and $m = 3.5 \text{ MeV}$. The quark condensate is $(\langle \bar{\psi}\psi \rangle)^{1/3} = -282.4 \text{ MeV}$. Then we have $G' = 4.1433 \times 10^{-6} \text{ MeV}^{-2}$, and $\tau_{UV} = 955 \text{ MeV}$. At a zero temperature, the quark number density is given by

$$\rho_{u,d} = 2N_c \int \frac{d^3p}{(2\pi)^3} \theta(\mu_r - E_p). \quad (18)$$

The quark pressure and energy density for quark matter are given by [51, 52]

$$\varepsilon(\mu_u, \mu_d) = -P(\mu_u, \mu_d) + \sum_{u,d} \mu\rho(\mu), \quad (19)$$

$$P(\mu_u, \mu_d) = P_0 + \sum_{u,d} \int_0^\mu d\mu\rho(\mu). \quad (20)$$

Here, P_0 represents the vacuum pressure density at $\mu = 0$. In many works, P_0 is taken as a free parameter corresponding

to the bag constant in the MIT bag model, or defined as the pressure difference between Nambu phase and Wigner phase in the case of chiral limit. Here we take $P_0 = -(140 \text{ MeV})^4$. We include the electron to guarantee the local neutrality of electric charge with

$$\frac{2}{3}\rho_u - \frac{1}{3}\rho_d - \rho_e = 0. \quad (21)$$

Using μ_e to denote the electron-charge chemical potential and treating the electron as ideal Fermi gas, the electron density is given by

$$\rho_e = \frac{\mu_e^3}{3\pi^2}. \quad (22)$$

The total baryon number density is $\rho^Q = (\rho_u + \rho_d)/3$. The chemical potentials satisfy the weak equilibrium $d \leftrightarrow u + e + \bar{\nu}_e$ which gives

$$\mu_d = \mu_u + \mu_e. \quad (23)$$

Then the pressure and energy density of the quark matter are

$$\varepsilon^Q = \varepsilon(\mu_u, \mu_d) + \frac{\mu_e^4}{4\pi^2}, \quad (24)$$

$$P^Q = P(\mu_u, \mu_d) + \frac{\mu_e^4}{12\pi^2}, \quad (25)$$

respectively. With a fixed pressure of vacuum P_0 , the stiffness of EOS increases along with α .

C. Construction for the phase transition

Commonly there are two methods to mix the quark phase and hadron phase by requiring the chemical, thermal, and mechanical equilibrium. The Gibbs construction. With a volume fraction χ of the quark phase, it only requires the charge neutrality to be fulfilled globally. In this construction, the pressure of mixed phase continuously increase with the baryon number density. The Maxwell construction. It requires the local electrical neutrality. The EOS can be obtained independently. At the phase transition point the two different phases have same chemical potential, temperature, and pressure with $\mu^H = \mu^Q$, $P^H = P^Q$, and $n_q^H = n_q^Q = 0$, where n_q is the local electric charge density. It is different from Gibbs construction that the two phases at the phase transition point have different baryon number density. It is expected for star with spherical symmetry that the pressure is a continuous function of radius and thus of baryon density. Furthermore, this construction means a very large hadron-quark surface tension and leads to a first order phase transition between hadron and quark phases.

How the nature of the phase transition depends on the surface tension still remains unclear. Based on the analysis of the two methods above, to get the hybrid EOS in this paper, we try to use an interpolating approach to connect the hadron and quark EOS. Specifically, we adopt the P-interpolation in $P - \mu$ plane. In this method, the pressure and energy density

of hybrid EOS are give by

$$P(\mu) = P^H(\mu)f_-(\mu) + P^Q(\mu)f_+(\mu), \quad (26)$$

$$\varepsilon(\mu) = \varepsilon^H(\mu)f_-(\mu) + \varepsilon^Q(\mu)f_+(\mu) + \Delta\varepsilon, \quad (27)$$

with

$$f_{\pm}(\mu) = \frac{1}{2} \left(1 \pm \tanh \left(\frac{\mu - \mu_c}{\Gamma} \right) \right), \quad (28)$$

$$\Delta\varepsilon = \frac{2\mu}{\Gamma} (P^Q - P^H) (e^X + e^{-X})^{-2}, \quad (29)$$

$$X = \frac{\mu - \mu_c}{\Gamma}. \quad (30)$$

The function f_{\pm} is a sigmoid function which has similar role as the χ in the Gibbs construction and realize a smooth EOS in the interval of $(\mu_c - \Gamma, \mu_c + \Gamma)$. The additional term $\Delta\varepsilon$ guarantees thermodynamic consistency. The pressure (P^H , P^Q) and energy density (ε^H , ε^Q) can be derived separately at the hadron phase and quark phase. But for the hybrid EOS, two free parameters, $\bar{\mu}$ and Γ , remain to be determined. As showed in Figure 1, when Γ approaches zero, the smooth EOS transitions to a discontinuous EOS that is a result of Maxwell construction.

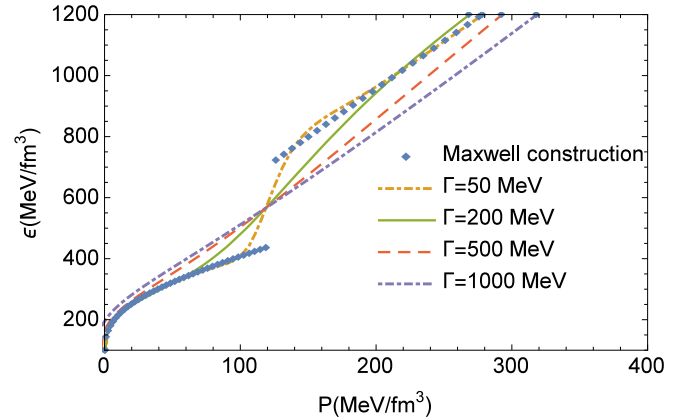


FIG. 1: EOSs at $\alpha=0.5$ for different interpolating interval Γ . The Maxwell construction of hybrid EOS corresponds to $\Gamma = 0$. The influence of Γ on the stiffness of EOS at the two sides of μ_c are different.

III. RESULTS AND ANALYSIS

A. The hybrid EOS

The quark chemical potential related to baryon chemical potentials can be written in detail as any of the following equations:

$$\mu_u = (\mu_n - 2\mu_e)/3, \quad (31)$$

$$\mu_d = (\mu_n + \mu_e)/3, \quad (32)$$

$$\mu_n = \mu_u + 2\mu_d, \quad (33)$$

where μ_n is the baryon chemical potential of neutron.

In the sigmoid function $f_{\pm}(\mu)$ of Eq. (28), $\mu_c - \Gamma$ sets the beginning of deconfinement of quark. The parameter Γ affects the stiffness of the EOS. For an illustration, we plot the EOS of $\alpha = 0.5$ for different Γ 's in Figure 1. There is a jump for $\Gamma = 0$, but not for large enough Γ . As shown in Figure 1 for $\Gamma \geq 50$ MeV, all lines of hybrid EOS smoothly increase with pressure and have an intersection at the equilibrium pressure defined in Maxwell construction. As Γ gets larger than 1 GeV, the hyperbolic tangent function approaches zero, then the two phases will have equal weights. Thus, it is important to set constraints on the possible values of Γ . However, in our NJL model only chiral transition is studied, whose relation with deconfinement transition is unclear. Some studies [53, 54] suggest that the transition starts at roughly 1 GeV. So, it set constraint on Γ with $\Gamma < \mu - 1$ GeV.

The baryon density and pressure of the hadron matter is $2.67 \rho_0$ and $108 \text{ MeV}/fm^3$, respectively, at $\mu = 1300$ MeV and $2.98 \rho_0$ and $151 \text{ MeV}/fm^3$ at $\mu = 1400$ MeV. For the quark matter, the baryon density at $\mu = 1300(1400)$ MeV is about $4.5(5.6) \rho_0$ for different α with pressure range from 100 MeV to 400 MeV. An illustration of the interpolation in the $P - \mu$ plane is presented in Figure 2.

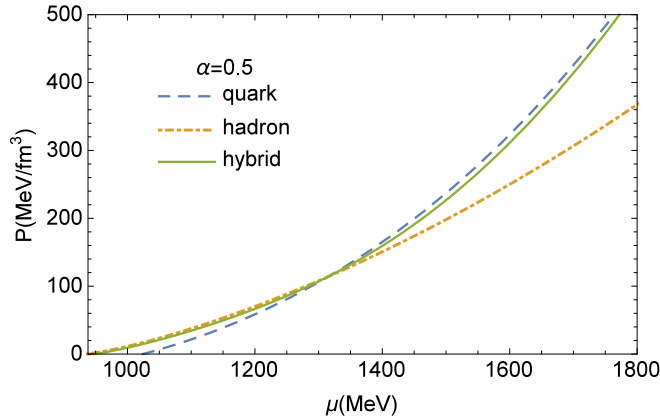


FIG. 2: An illustration of the EOS with pressure-interpolation. The transition can be realized smoothly in the region of $(\mu_c - \Gamma, \mu_c + \Gamma)$.

Plots of the energy density as function of pressure are presented in Figure 3. The interpolation width Γ has significant influences on the stiffness of hybrid EOS at the two sides of $\bar{\mu}$. At large Γ , the lines monotonically increase. When Γ is relatively small, the lines become non-monotonically increasing around $P = 150 \text{ MeV}/fm^3$ which is the pressure of hadron matter at $\mu = 1300$ MeV. The weighting parameter α has significant impact on the stiffness of hybrid EOS. The stiffness of quark EOS increases with α , but this only happens for small Γ at high pressure in the hybrid EOS. This confirms that the hadron EOS is dominant at low density.

To produce the EOS of Maxwell construction, it is not just to set $\Gamma = 0$ with arbitrary μ_c . We must find the intersection of the quark and hadron EOS in the $P - \mu$ plane. The transition chemical potential is 1215 MeV for $\alpha = 0.5$. We plot the EOS that corresponds to the one from Maxwell construction

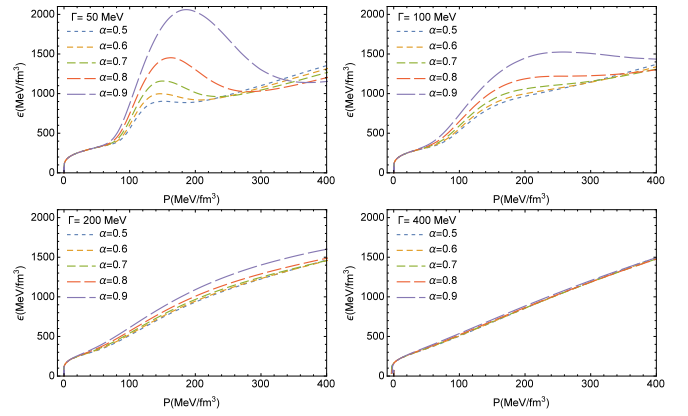


FIG. 3: Hybrid EOS for different interpolation width Γ at $\mu_c = 1300$ MeV. The results of different α begin to differentiate when Γ becomes smaller.

in Figure 4. For α larger than 0.5 at $\mu = 1215$ MeV, both energy density and pressure are discontinuous.

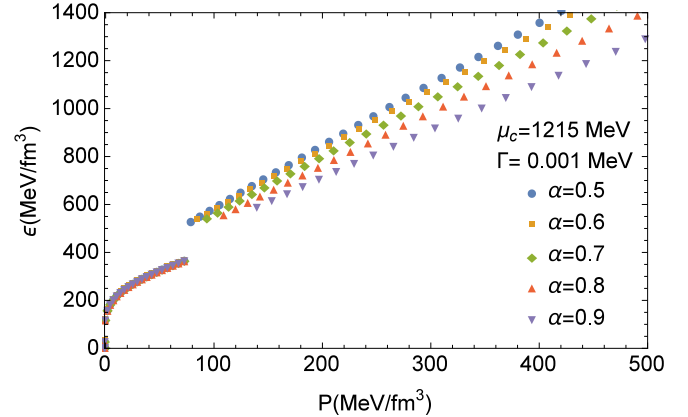


FIG. 4: Hybrid EOS for different α at $\mu_c = 1215$ MeV. In this case, the EOS from the interpolation method is corresponding to the EOS from Maxwell construction.

B. Mass-radius relations

We use the TOV equations (in units $G = c = 1$):

$$\frac{dP(r)}{dr} = -\frac{(\varepsilon + P)(M + 4\pi r^3 P)}{r(r - 2M)}, \quad (34)$$

$$\frac{dM(r)}{dr} = 4\pi r^2 \varepsilon, \quad (35)$$

to investigate the mass-radius relation.

The mass-radius relations are showed in Figure 5 which has several features. First of all, when the Γ and μ_c are fixed, the difference of hybrid EOS mainly lies in the difference of α , and then affects the mass radius relation. The maximum mass of hybrid stars increases with increasing α , which is different with that of pure quark stars. As shown in the upper-left

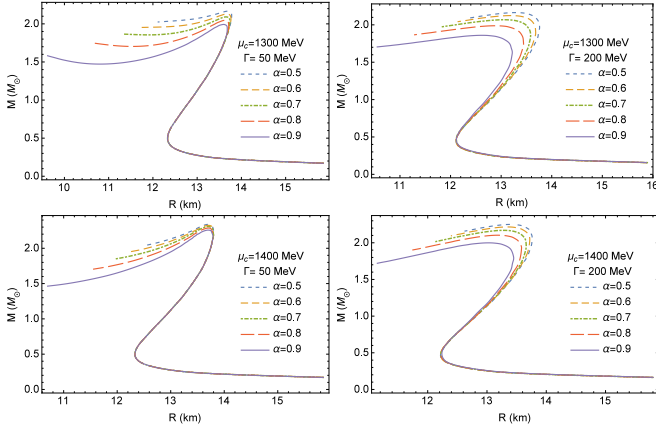


FIG. 5: The mass-radius relation for different α , Γ , and μ_c .

picture in Figure 3, the hybrid EOS becomes softer with increasing α in the middle region of pressure. Second, we use the harder EOS of hadron matter that neutron star can have maximum mass about $2.7 M_\odot$. In the Figure 5, the maximum mass of the hybrid star appears below $2.5 M_\odot$. The curves almost coincide with each other in low mass regions, but separate with the change of α in high mass regions. This shows that for hybrid stars from our model, hadron matter dominates in low mass stars, while for high mass stars, quark matter has a great influence on the star mass. Third, when Γ is fixed, the maximum mass of the hybrid star increases with increasing chemical potential μ_c . When μ_c is fixed, quark matter and hadron matter can be mixed in a larger chemical potential region with increasing Γ . This is reflected in the Figure 5 where the curves begin to separate at a smaller mass. Lastly, in the upper-left picture of Figure 5, it seems that mass twin phenomenon appears for larger α when extending the curves. But the energy density and pressure of the hybrid EOS given by our model is not high enough. We need to do further analysis on this point.

In Figure 5, the radius for a $1.4 M_\odot$ star is less than the constraints $R \leq 13.76$ km or $R \leq 13.6$ km [55, 56] and larger than 10.7 km [57]. Although these radius constraints are model-dependent and may not suitable for hybrid stars, we still present here as a comparison.

C. Tidal deformability

In the early works of Ref. [19, 58], restrictions on the tidal deformability for a $1.4 M_\odot$ is less than 800 (1400) for low (high) –spin prior case. The most recently analysis in analysis on the binary neutron star merger GW170817 have found tighter constraints on the component mass to lie between 1.00 and $1.89 M_\odot$ with $\tilde{\Lambda}$ in $(0, 630)$ when allowing for large component spins and on the component masses to lie between 1.16 and $1.60 M_\odot$ with $\tilde{\Lambda} = 300^{+420}_{-230}$ when the spins are restricted to be within the range observed in Galactic binary neutron stars [59].

The $\tilde{\Lambda}$ is a mass-weighted linear combination of the two

tidal parameters Λ_1 and Λ_2 . With M_1 and M_2 the corresponding gravitational masses, the $\tilde{\Lambda}$ is defined as

$$\tilde{\Lambda} = \frac{16 (M_1 + 12M_2)M_1^4\Lambda_1 + (M_2 + 12M_1)M_2^4\Lambda_2}{13 (M_1 + M_2)^5}. \quad (36)$$

In deducing the $\tilde{\Lambda}$ in the low-spin case, the component mass have being constrained to $M_1 \in (1.16, 1.36) M_\odot$ and $M_2 \in (1.36, 1.60) M_\odot$ with total mass $2.73^{+0.04}_{-0.01} M_\odot$ and chirp mass $1.186^{+0.001}_{-0.001} M_\odot$. The chirp mass is defined as

$$M_{chirp} = \frac{(M_1 M_2)^{3/5}}{(M_1 + M_2)^{1/5}} \quad (37)$$

In the calculation of tidal deformability Λ , one way is to use a universal relation only between Λ and compactness $C = M/R$ with M and R being the star mass and radius respectively [60, 61]. But here, we calculate Λ through the compactness and the Love number. The tidal deformability is related to the $l = 2$ dimensionless tidal Love number k_2 through

$$k_2 = \frac{3}{2} \Lambda \left(\frac{M}{R} \right)^5 \quad (38)$$

in units $G = c = 1$. The $l = 2$ tidal Love number k_2 for the internal solution is given by [62]

$$k_2 = \frac{8}{5} C^5 (1 - 2C)^2 [2 + 2C(y - 1) - y] \times \{2C[6 - 3y + 3C(5y - 8)] + 4C^3[13 - 11y + C(3y - 2) + 2C^2(1 + y)] + 3(1 - 2C)^2[2 - y + 2C(y - 1)] \ln(1 - 2C)\}^{-1}, \quad (39)$$

in matching the interior and exterior solutions across the star surface. Here, y is related to the metric variable H and surface energy density ϵ_0

$$y = \frac{R\beta(R)}{H(R)} - \frac{4\pi R^3 \epsilon_0}{M}. \quad (40)$$

For some neutron star model the surface energy density is zero. But in our NJL model with negative vacuum pressure, the surface energy ϵ_0 is nonzero. So the last term can not be neglected.

The metric variable H related to the EOS can be obtained by integrating two differential equations

$$\frac{dH(r)}{dr} = \beta, \quad (41)$$

$$\frac{d\beta(r)}{dr} = 2gH\{-2\pi[5\epsilon + 9P + f(\epsilon + P)] + \frac{3}{r^2} + 2g(\frac{M}{r^2} + 4\pi rP)^2\} + 2g\frac{\beta}{r}[-1 + \frac{M}{r} + 2\pi r^2(\epsilon - P)], \quad (42)$$

where $g = (1 - 2M/r)^{-1}$ and $f = d\epsilon/dP$. The iteration start from the center at $r = 0$ via expansions $H(r) = a_0 r^2$ and $\beta(r) = 2a_0 r$ with constant a_0 . As can be seen from Eq. (40), we only concern the ratio β/H . So a_0 can be arbitrarily chosen in numerical calculation.

TABLE I: Results of tidal deformability with mass constraints from Ref. [59] in the low-spin case. Here, the parameters in the interpolation are $\Gamma = 50$ MeV and $\mu_c = 1300$ MeV.

$M_1(M_\odot)$	$M_2(M_\odot)$	Λ_1	Λ_2	$\tilde{\Lambda}$
1.160	1.609	1952.10	371.394	839.237
1.326	1.400	1027.41	768.748	888.738
1.362	1.363	887.325	883.712	885.517

In Table I, we show the calculated Λ and $\tilde{\Lambda}$ for masses satisfying the mass constraints given above, i.e., $M_1 \in (1.16, 1.36) M_\odot$ and $M_2 \in (1.36, 1.60) M_\odot$ with total mass $2.73_{-0.01}^{+0.04} M_\odot$ and chirp mass $1.186_{-0.001}^{+0.001} M_\odot$. To include the boundary and mass of $1.4 M_\odot$, we design three sets of mass as shown in the table. First, we choose a narrow width $\Gamma = 50$ MeV with $\mu_c = 1300$ MeV. As shown in Figure 5, for the mass between (1.16, 1.60) the curve does not show a dependence on α , so the hybrid stars are dominated by hadron matter in this mass range. The calculated results of $\tilde{\Lambda}$ in Table I are out of the range 300_{-230}^{+420} in the low-spin case.

Then we take a larger value of Γ . When Γ is increased, quark matter and hadron matter are considered to mix in a larger region in the $P - \mu$ plane. We can find in Table II that the calculated tidal deformabilities are within 300_{-230}^{+420} from analysis on the binary neutron star merger GW170817. In Table III, we also give results when Γ is increased further. Compared with the results in Table II, the tidal deformabilities $\tilde{\Lambda}$ are obviously reduced but still within the allowed range. The results are more close to the center value.

TABLE II: Results of tidal deformability with $\Gamma = 300$ MeV and $\mu_c = 1300$ MeV for different α . Here, the labels a, b, and c indicate the three sets of component mass as listed in Table I.

α	$\tilde{\Lambda}_a$	$\tilde{\Lambda}_b$	$\tilde{\Lambda}_c$
0.5	482.991	515.836	517.420
0.6	475.476	518.318	520.031
0.7	474.121	507.478	506.659
0.8	470.32	503.15	506.235
0.9	459.558	490.097	492.191

IV. SUMMARY

Investigation of QCD matter transition at low temperature and high baryon chemical potential relies heavily on effective models for lacking data from experiment. Among it, a

TABLE III: Results of tidal deformability at $\alpha = 0.5$ with interpolation parameters $\Gamma = 500$ MeV and $\mu_c = 1300$ MeV.

$M_1(M_\odot)$	$M_2(M_\odot)$	Λ_1	Λ_2	$\tilde{\Lambda}$
1.160	1.609	753.687	151.865	330.689
1.326	1.400	406.400	304.145	351.581
1.362	1.363	351.925	354.034	352.981

construction connecting the hadron and quark phases is indispensable. There are two commonly used criteria for the phase transition in construct a hybrid EOS, i.e., the Gibbs construction and the Maxwell construction. During the hadron-quark transition, the baryon number density changes continuously by using the Gibbs construction, but not continuously with the Maxwell construction. Since the transition still remains uncertain experimentally, we take P -interpolation on the $P - \mu$ plane to get the EOS of hybrid stars. This method, depending on the central baryon chemical potential of interpolating area $\bar{\mu}$ and half of the interpolating interval Γ , gives a smooth EOS.

We use Walecka's RMF theory to describe the nuclear phase and use our recently developed NJL model to describe the quark phase. We have tried two sets of parameters (TM1 and NL3) in the RMF theory and found only the NL3 parameter set can be used in our analysis. At the quark level, we have two parameters in adjusting the EOS. It is the vacuum pressure P_0 and the parameter α that weights the contribution from the vector channel in the Fierz-transformed Lagrangian.

We have studied the dependence of hybrid EOS and mass-radius relation on $\bar{\mu}$ and Γ . The results show that the stiffness of the EOS and maximum mass given by the hybrid EOS are sensitive to $\bar{\mu}$ and Γ . In this paper, we use the possible deconfinement chemical potential and baryon chemical potential equilibrium to fix $\bar{\mu}$ and Γ . Parameters $\bar{\mu}$ and Γ as a function of α give the area of mixed phases. The central baryon density is about $3 \rho_0$ for hadron matter and about $4.5 \rho_0$ for quark matter, where ρ_0 is the saturation density of nuclear matter.

The stiffness of hybrid EOS increases with α . By adjusting α , maximum mass of hybrid stars can be larger than masses from PSR J1614-2230 ($M = 1.928 \pm 0.017 M_\odot$) [16] and PSR J0348+0432 ($M = 2.01 \pm 0.04 M_\odot$) [17] and the recent observation of MSP J0740+6620 with star mass $2.14_{-0.09}^{+0.10}$ within the 68.3 credibility interval [18]. The calculated radii of a 1.4-solar-mass star for two different quark vacuum pressures are less than $R \leq 13.76$ km or $R \leq 13.6$ km from Refs. [55, 56] which are model-dependent constrains. The lower limit 10.7 km of a 1.6-solar-mass neutron star is also satisfied. In a recent analysis on the binary neutron star merger GW170817, the tidal deformability is $\Lambda = 300_{-230}^{+420}$ for the component masses to lie between $1.16 M_\odot$ and $1.60 M_\odot$ when the spins are restricted [59].

When the interpolation area of the two phases is narrow, mass-twin phenomenon that have been found in the Maxwell construction seems to appear in the mass-radius plot. But under the current parameter choices, the core energy of stars can not reach the required high value. Moreover, in the mass range

of $(1.16, 1.36) M_{\odot}$, the stars are mainly of hadron matter. The calculated tidal deformabilities $\tilde{\Lambda}$ do not satisfy the results in Ref. [59]. When Γ is increased, we have found that the calculated $\tilde{\Lambda}$ are in the range $\Lambda = 300^{+420}_{-230}$ of low spin case. The results are better when Γ increases further. So, EOS of pure hadron phase or hybrid phase with Maxwell construction can be excluded by the observation of tidal deformability from GW170817, but hybrid phase with a crossover transition may be still suggested to be effective to describe the phase in hybrid star.

Acknowledgments

This work is supported in part by the National Natural Science Foundation of China (under Grants No. 11475085, No. 11535005, No. 11690030, No.11873030, and No. 11905104) and the National Major state Basic Research and Development of China (Grant No. 2016YFE0129300).

-
- [1] M. Buballa, Phys. Rep. **407**: 205 (2005)
- [2] K. Rajagopal, F. Wilczek, "At the Frontier of Particle Physics / Handbook of QCD", Vol. 3 (World Scientific, 2001)
- [3] X. F. Luo, and N. Xu, Nucl. Sci. Tech. **28**: 112 (2017)
- [4] Y. Aoki, G. Endrodi, Z. Fodor, S. D. Katz, K. K. Szabo, Nature (London) **443**: 675 (2006)
- [5] G. S. Bali, F. Bruckmann, G. Endrodi, Z. Fodor, S. D. Katz, and A. Schafer, Phys. Rev. D, **86**: 071502(R) (2012)
- [6] J. Braun, L. M. Haas, F. Marhauser, and J. M. Pawłowski, Phys. Rev. Lett., **106**: 022002 (2011)
- [7] S. Typel, Phys. Rev. C, **71**: 064301 (2005)
- [8] B. J. Schaefer, J. M. Pawłowski and J. Wambach, Phys. Rev. D, **76**: 074023 (2007)
- [9] G. Y. Shao, M. Di Toro, V. Greco et al, Phys. Rev. D, **84**: 034028 (2011)
- [10] Y. Sakai, T. Sasaki, H. Kouno, and M. Yahiro, J. Phys. G, **39**: 035004 (2012)
- [11] E. R. Most, L. J. Papenfort, V. Dexheimer et al, Phys.Rev.Lett., **122**: 061101 (2019)
- [12] M. G. Orsaria, G. Malfatti, M. Marianio et al, J. Phys. G, **46**: 073002 (2019)
- [13] M. Hanauske, L. Bovard, E. Most et al, Universe, **5**: 156 (2019)
- [14] A. Bauswein, Niels-Uwe F. Bastian, D. B. Blaschke et al, Phys. Rev. Lett., **122**: 061102 (2019)
- [15] P. Demorest, T. Pennucci, S. M. Ransom, M. S. E. Roberts, and J. W. T. Hessels, Nature **467**: 1081-3 (2010)
- [16] E. Fonseca, T. T. Pennucci, J. A. Ellis et al, Astrophys. J., **832**: 167 (2016)
- [17] J. Antoniadis, P. C. C. Freire, N. Wex et al, Science, **340**: 6131 (2013)
- [18] H. T. Cromartie, E. Fonseca, S. M. Ransom et al, Nat. Astron., **4**: 72 (2019)
- [19] B. P. Abbott, R. Abbott, T. D. Abbott et al, (LIGO Scientific and Virgo Collaborations), Phys.Rev. Lett., **119**, 161101 (2017)
- [20] E. Witten, Phys. Rev. D, **30**: 272 (1984)
- [21] A. R. Bodmer, Phys. Rev. D, **4**: 1601 (1971)
- [22] H. Terazawa, J. Phys. Soc. Jpn., **58**: 3555 (1989); **58**: 4388 (1989); **59**: 1199 (1990)
- [23] B. Holdom, J. Ren, and C. Zhang, Phys. Rev. Lett., **120**: 222001 (2018)
- [24] Q. Y. Wang, T. Zhao, and H. S. Zong, arXiv: 1908.01325 (2019)
- [25] N. K. Glendenning, S. A. Moszkowski, Phys. Rev. Lett., **67**: 2414 (1991)
- [26] P. K. Panda, D. P. Menezes, C. Providencia, Phys. Rev. C, **69**, 025207 (2004)
- [27] J. Xu, L. W. Chen, C. M. Ko, B. A. Li, Phys. Rev. C, **81**: 055803 (2010)
- [28] G. Montana, L. Tolos, M. Hanauske, and L. Rezzolla, Phys. Rev. D, **99**: 103009 (2019)
- [29] B. P. Abbott, R. Abbott, T. D. Abbott *et al.*, (Virgo and LIGO Scientific Collaborations), Phys. Rev. Lett., **116**: 061102 (2016)
- [30] N. K. Glendenning, "Compact stars", Springer, New York, (1997)
- [31] Y. Yan, J. Cao, X. L. Luo, W. M. Sun, and H. Zong, Phys. Rev. D, **86**: 114028 (2012)
- [32] S. Benic, D. Blaschke, D. E. Alvarez-Castill et al, Astron. Astrophys., **577**: A40 (2015)
- [33] U. H. Gerlach, Phys. Rev., **172**: 1325 (1968)
- [34] M. A. R. Kaltenborn, Niels-Uwe F. Bastian, D. B. Blaschke, Phys. Rev. D, **96**: 056024 (2017)
- [35] D. Blaschke, H. Grigorian, and D. N. Voskresensky, Phys. Rev. C, **88**: 065805 (2013)
- [36] D. E. Alvarez-Castillo and D. Blaschke, Phys. Part. Nucl., **46**: 846 (2015)
- [37] M. G. Alford, S. Han, and M. Prakash, Phys. Rev. D, **88**: 083013 (2013)
- [38] J. Macher and J. Schaffner-Bielich, Eur. J. Phys., **26**: 341 (2005)
- [39] G. Baym et al, Rep. Prog. Phys. **81**, 056902 (2018)
- [40] Q. Y. Wang, T. Zhao, and H. S. Zong, arXiv: 1908.01325 (2019)
- [41] F. Wang, Y. Cao, and H. Zong, Chin. Phys. C, **43**: 084102 (2019)
- [42] T. Zhao, W. Zheng, F. Wang, C. M. Li, Y. Yan, Y. F. Huang, and H. S. Zong, Phys. Rev. D, **100**: 043018 (2019)
- [43] Q. Wang, C. Shi, and H. S. Zong, Phys. Rev. D, **100**: 123003 (2019)
- [44] G. Baym, C. Pethick, P. Sutherland, Astrophys. J., **170**: 299(1971)
- [45] J. Negele, D. Vautherin, Nucl. Phys. A **207**: 298 (1973)
- [46] N. K. Glendenning, Phys. Rev. C, **64**: 025801 (2001)
- [47] G. A. Lalazissis, J. König, P. Ring, Phys. Rev. C, **55**: 540 (1997)
- [48] Y. Sugahara, H. Toki, Nucl. Phys. A, **579**: 557 (1994)
- [49] S. P. Klevansky, Rev. Mod. Phys., **64**: 649 (1992)
- [50] T. Kunihiro and R. Hatsuda, Prog. Theor. Phys., **74**: 765 (1985)
- [51] H. S. Zong, W. M. Sun, Phys. Rev. D, **78**: 054001 (2008)
- [52] H. S. Zong, W. M. Sun, Int. J. Mod. Phys. A, **23**: 3591 (2008)
- [53] K. Fukushima, Phys. Rev. D, **77**: 114028 (2008)
- [54] K. Fukushima and T. Hatsuda, Rep. Prog. Phys., **74**: 014001 (2011)
- [55] F. J. Fattoyev, J. Piekarewicz, and C. J. Horowitz, Phys. Rev. Lett., **120**: 172702 (2018)
- [56] E. Annala, T. Gorda, A. Kurkela, and A. Vuorinen, Phys. Rev. Lett., **120**: 172703 (2018)
- [57] A. Bauswein, AIP Conf. Proc., **2127**: 020013 (2019)
- [58] B. Margalit and B. D. Metzger, Astrophys. J. Lett., **850**: L19 (2017)
- [59] B. P. Abbott, R. Abbott, T. D. Abbott et al, (LIGO Scientific and Virgo Collaborations), Phys. Rev. X, **9**: 011001 (2019)

- [60] Z. Carson, K. Chatziioannou, C.-J. Haster, K. Yagi, and N. Yunes, *Phys. Rev. D*, **99**: 083016 (2019)
- [61] H. -Y. Chen, P. M. Chesler, and A. Loeb, arXiv:1909.04096
- [62] T. Damour and A. Nagar, *Phys. Rev. D*, **80**: 084035 (2009)